Supporting Information

Electrochemical catalyst-support effects and their stabilizing role for IrO_x nanoparticle catalysts during the oxygen evolution reaction (OER)

Hyung-Suk Oh [a], Hong Nhan Nong [a], Detre Teschner [b], Tobias Reier [a], Arno Bergmann [a], Manuel Gliech [a], Jorge Ferreira de Araújo [a], Elena Willinger [b], Robert Schlögl [b] and Peter Strasser [a]*

[a] *The Electrochemical Energy, Catalysis, and Materials Science Laboratory, Department of Chemistry, Chemical Engineering Division, Technical University Berlin, Berlin 10623, Germany*

[b] *Fritz-Haber-Institut der Max-Planck-Gesellschaft, Abteilung Anorganische Chemie, Berlin 14195, Germany*

Supporting Information contains:

- ***The preparation of antimony doped tin oxide (ATO) support***
- ***Differential Electrochemical Mass Spectrometry (DEMS) study of IrO_x supported on ATO***

Figure S1: *XRD patterns of (a) synthesized antimony doped tin oxide (ATO) and (b) Ir nanoparticles supported on ATO.*

Figure S2: *High-resolution TEM images of Ir nanoparticles supported on (a) carbon black and (b) commercial antimony doped tin oxide (Com. ATO).*

Figure S3: *Low-magnification TEM images of Ir nanoparticles supported on (a) carbon black, (b) commercial antimony doped tin oxide (Com. ATO) and synthesized ATO.*

Figure S4. *High-resolution HAADF images after high electron beam-dose.*

Figure S5. *A curve fitting analysis of XANES by using a set of arctangent function (blue doted line) and Lorentzian function (green solid line) in Athena program. The dots show the experimental spectrum and the red solid lines show the simulated curve: (a) Ir foil, (b) commercial $IrCl_3$, (c) precalcined commercial IrO_2, (d) IrO_x/C, (e) IrO_x/Com. ATO and (f) IrO_x/ATO.*

Figure S6. *Simultaneously recorded cyclic voltammgorams (CV) and mass spectrometric cyclic voltammograms (MSCV) for oxygen evolution reaction (OER) in N_2 saturated 0.05 M H_2SO_4 solution in the* dual thin-layer electrochemical flow cell. *(a) bulk IrO_x, (b) IrO_x/C, (c) IrO_x/Com. ATO and (d) IrO_x/ATO.*

Figure S7. *10 $mAcm^{-2}$ constant current-load stability test of IrO_x/ATO electrocatalysts for OER. For comparision, IrO_x/C and IrO_x/Com. ATO measured under same condition. Ir electrocatalyst loading 10.2 $\mu g\ cm^{-2}$, N_2 purged 0.05 M H_2SO_4 (pH 1), 1600 rpm, room temperature.*

Figure S8. *EDS patterns of IrO_x nanoparticles supported on (a) carbon black, (b) commercial ATO and (c) synthesized ATO after stability test.*

Figure S9. *Ir-mass loss ratio of IrO_x/C, IrO_x/Com. ATO and IrO_x/ATO after stability test based on the initial Ir mass. Red and Green portions indicate the nature of the Ir loss, by detachment or by dissolution.*

Figure S10. *Ir-mass based activity at η = 280 mV overpotential of IrO_x/C, IrO_x/Com. ATO and IrO_x/ATO before and after stability test.*

Figure S11: *TEM images of IrO_x nanoparticles supported on (a) carbon black, (b) commercial ATO and (c) synthesized ATO before and after stability test.*

Figure S12. *Nyquist plots of commercial IrO_2, IrO_x/C, IrO_x/Com. ATO and IrO_x/ATO at 1.7 V_{RHE}, Ir electrocatalyst loading 10.3 $\mu g\ cm^{-2}$, N_2 purged 0.05 M H_2SO_4 (pH 1), 1600 rpm, room temperature, frequency range 1 Hz ~ 100 kHz.*

Figure S13. *Nyquist plots of (a) IrO_x/C and (b) IrO_x/ATO at 1.7 V_{RHE} with different Ir electrocatalyst loading (10, 3, 1 and 0.3 $\mu g\ cm^{-2}$). (c) Charge trasfer resistance of IrO_x/C and IrO_x/ATO as a function of Ir electrocatalyst loading.*

Figure S14. *Tafel plots of (a) IrO_x/C and (b) IrO_x/ATO with different Ir electrocatalyst loading (10, 3, 1 and 0.3 $\mu g\ cm^{-2}$). N_2 purged 0.05 M H_2SO_4 (pH 1), scan rate 5 $mV\ s^{-1}$, 1600 rpm, room temperature, To calculate the tafel slope, 12 data points took in iR-corrected 1.45 ~ 1.60 V_{RHE}.*

The preparation of antimony doped tin oxide (ATO) support

Antimony doped tin oxide (ATO) was synthesized using sol-gel combinced hydrothermal methode in our previous work. [1] The synthesis mechanism are shown bellow.

First step: Tin tetrachloride ($SnCl_4$) and antimony acetate ($(CH_3CO_2)_3Sb$) reacted with ethanol solution and converted to the tin ethoxide and antimony ethoxide, respectively.

$$SnCl_4 + 4\,CH_3CH_2OH \rightarrow Sn(OC_2H_5)_4 + 4\,HCl \quad (E1)$$

$$Sb(CH_3CO_2)_3 + 3\,CH_3CH_2OH \rightarrow Sb(OC_2H_5)_3 + 3\,CH_3COOH \quad (E2)$$

Second step: Ammonium hydroxide hydrolyzed the ethoxides and the white suspended precipitate was shown in the second-order hydrolysis step. [2]

$$Sn(OC_2H_5)_4 + 2H_2O \rightarrow Sn(OH)_2(OC_2H_5)_2\downarrow + 2C_2H_5OH \quad (E3)$$

$$Sb(OC_2H_5)_3 + 2H_2O \rightarrow Sb(OH)_2(OC_2H_5)\downarrow + 2C_2H_5OH \quad (E4)$$

In the ethanol solution, the polar product is precipitated much more readily, and the size of the particles is smaller because of the solubility of polar compound in organic solvent is much lower than that in water.

Third step: The hydrolyzed ethoxides condensed during refluxing and hydrothermal process. In the hydrothermal step, the antimony elements were easy to incorporate into SnO_2 lattice and endow the nanocrystals with electrical conductivity. The TDA template is thermally decomposed in air condition and then left the mesopore into ATO structure.

Differential Electrochemical Mass Spectrometry (DEMS) study of IrO_x supported on ATO

DEMS experiments were recorded using a home designed dual thin-layer electrochemical flow cell partly based the original design reported elsewhere. [3] The gas products from the flow cell were detected using a PrismaTM quadrupole mass spectrometer (QMS 200, Pfeiffer-Vacuum) with two turbomolecular pumps (HiPace 80) operating under 10^{-6} mbar. The electrolyte was separated from the chamber by a 150 µm thick hydrophobic PTFE membrane (Cat. No. PF-003HS for Cobetter® porous size 30 nm). The working electrode (WE) has an exposed area of ~ 0.196 cm^2 and pressured against a Teflon gasket to form a thin layer with defined thickness around 100 µm. A Pt-mesh was used as counter electrode (CA) connected to tangential channel to main inlet channel and a leak-free Ag/AgCl reference electrode. The bulk catalyst Ir electrode was polished with silica slurries (Buehler) of 0.1 µm and 0.05 µm in particle size. IrO_x supported on different type catalyst supports, such as carbon, commercial antimony doped tin oxide (ATO) and synthesized ATO, were homogenously dispersed by ultrasonication for 20 min, and droped onto a pre-defined area ~ 0.196 cm^2 with inert Teflon film coated on glassy carbon electrodes (Φ = 10 mm in, HTW GmbH). The glassy carbon electrodes were polished with silica slurries (Buehler) of 1 µm and 0.05 µm in particle size. The geometric metal loading was kept constant at ~ 10.2 $\mu g_{Ir}\ cm^{-2}$. The electrolyte flow speed was set at the out let flow cell with a needle valve with 5 µL s^{-1} and controlled during experiments with a liquid flow sensor Sensirion SLQ-QT500. Measurements were afterwards corrected for the uncompensated ohmic resistance determined by electrochemical impedance spectroscopy. The WE and Teflon gasket contact were purged with N_2 in order to avoid environment air into the reaction compartment or exchange with MS chamber. The cyclevoltammetric mass spectrometer (MSCV) curves were recorded during OER regime in selected potential windows at a scan-rate of 5 mVs^{-1}, with four selective channels recording m/z 32, 44 simultaneously with electrochemical measurements. Current step measurements by stepping in increased current steps were used to determine the calibration constant, which describes the relationship between the faradaic charge (QF) and the charge signal from mass spectrometric (QMS). The ion current has later related to faradic current and FE% calculated according to the following formula;

$$FE_j(\%) = \frac{Q_{MS,j} \cdot n_j}{Q_F \cdot K_j} \cdot 100 = \frac{Q_{F,j}^{DEMS}}{Q_F} \cdot 100 \quad \text{(E5)}$$

where represents the number of electrons transferred in the oxygen evolution reaction (= 4), the derived faradic mass spectrum charge is obtain from.

$$Q_{F,j}^{DEMS} = \frac{Q_{MS,j} \cdot n_j}{K_j^*} \quad \text{(E6)}$$

Only anodic currents were included in the integration limits, and the potential limits were selected from the onset of the oxygen evolution until the level of detected O_2 had returned to initial baseline level. To assure optimized detection of products during potential cycling as assessed with mass spectrometer, the ion source was calibrated using calibration protocol presented at Quadera software. The calibration mass spectrum and chamber baked before experiments allowing us achieve background stability and reproducibility. The molecules at ion source are bombarded by electrons having energies of about 80 eV. The amplification of the secondary electron multiplier (SEM) was setup to be around 3 orders of magnitude compare to Faraday detector.

Reference

[1] H. S. Oh, H. N. Nong and P. Strasser, Advanced Functional Materials 25 (2015) 1074.

[2] X. Zhang and F. Gan, Nanocrystals – Synthesis, Characterization and Applications, Chapter 9, 169.

[3] Z. Jusys, H. Massong, H. Baltruschat, Journal of the Electrochemical Society 146 (1999) 1093.

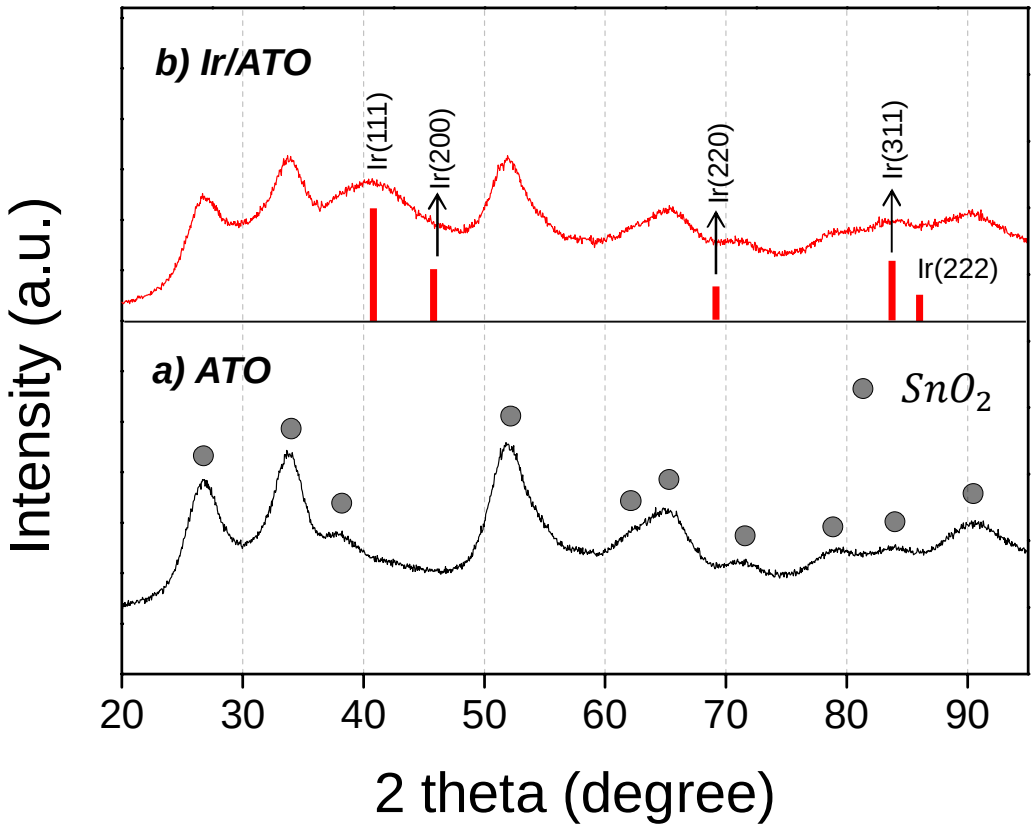

Figure S1. *XRD patterns of (a) synthesized antimony doped tin oxide (ATO) and (b) Ir nanoparticles supported on ATO.*

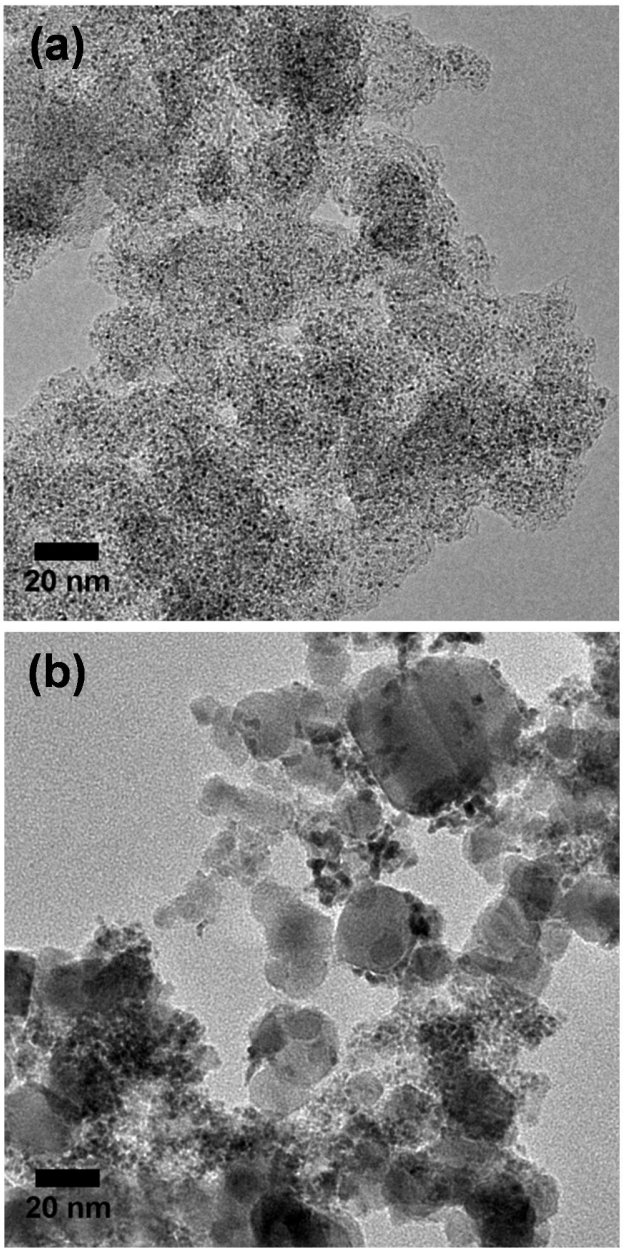

Figure S2. *High-resolution TEM images of Ir nanoparticles supported on (a) carbon black and (b) commercial antimony doped tin oxide (Com. ATO).*

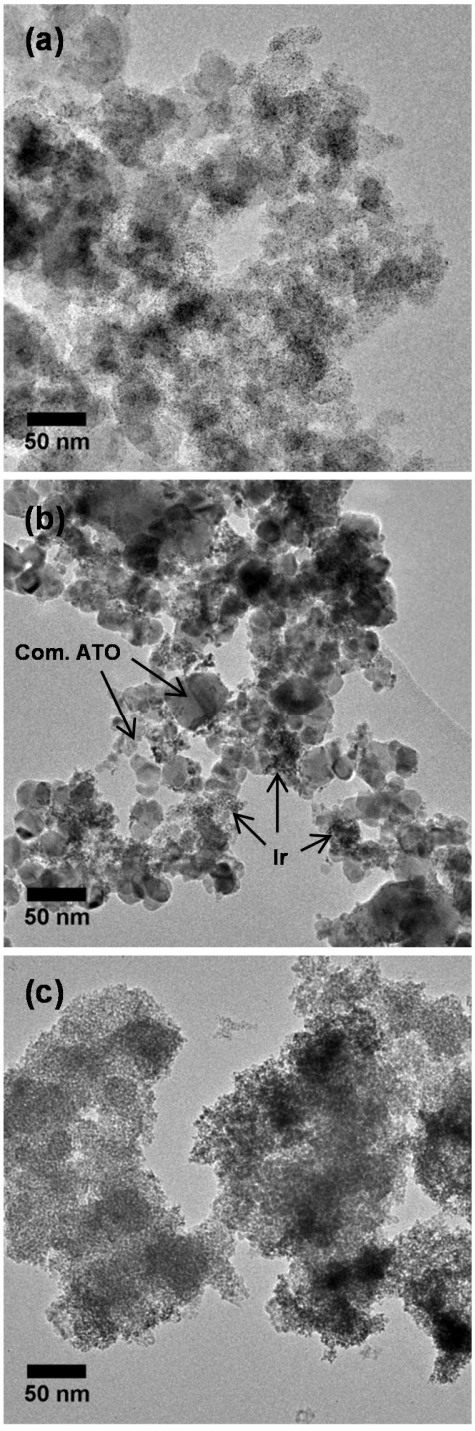

Figure S3. *Low-magnification TEM images of Ir nanoparticles supported on (a) carbon black, (b) commercial antimony doped tin oxide (Com. ATO) and synthesized ATO.*

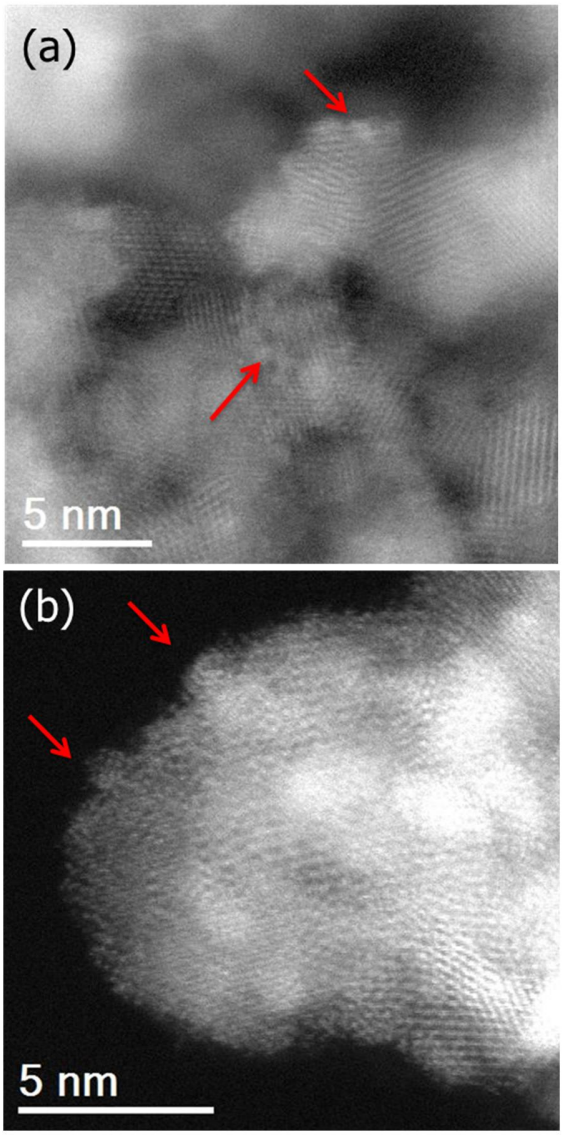

Figure S4. *High-resolution HAADF images after high electron beam-dose.*

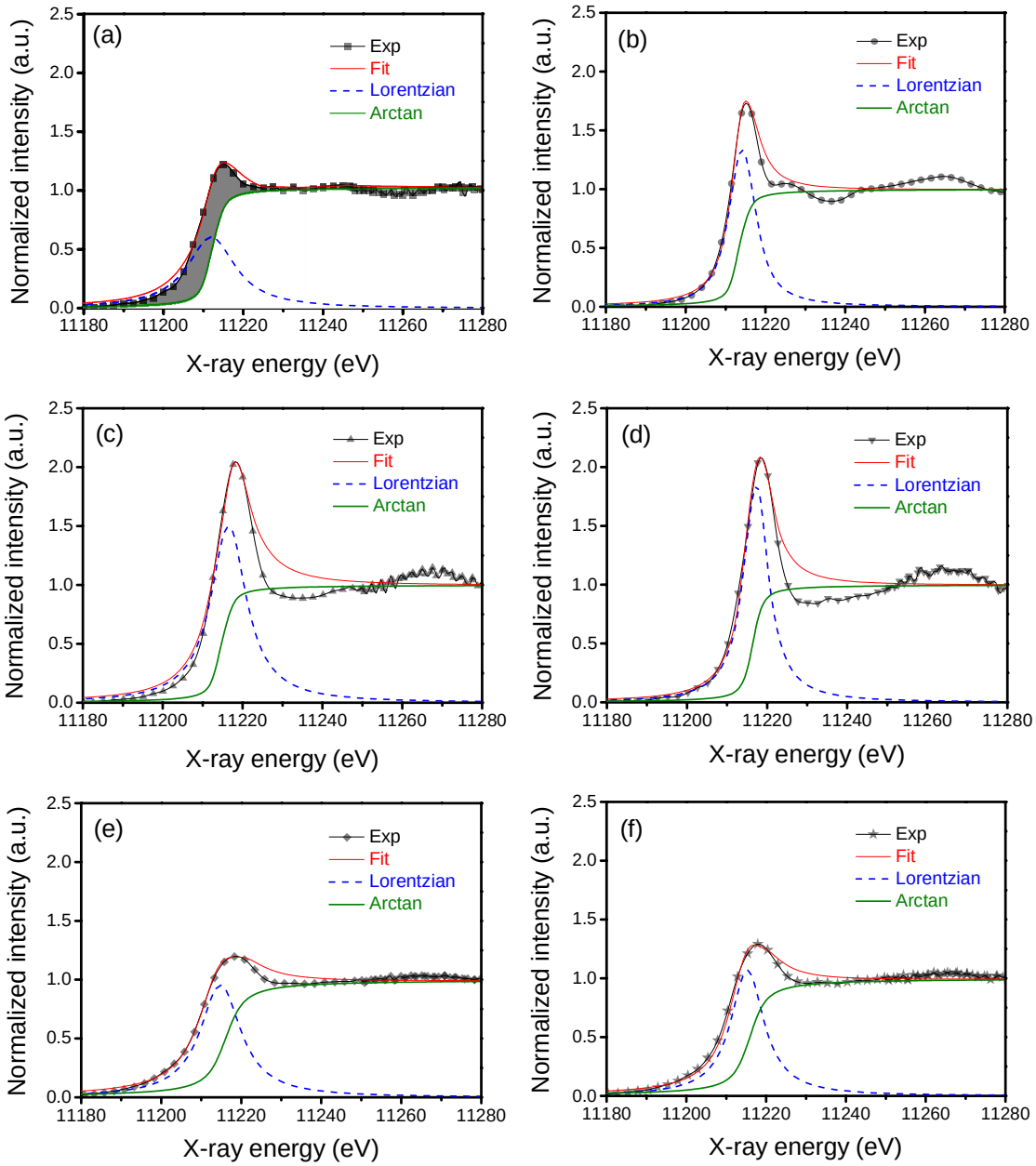

Figure S5. *A curve fitting analysis of XANES by using a set of arctangent function (blue doted line) and Lorentzian function (green solid line) in Athena program. The dots show the experimental spectrum and the red solid lines show the simulated curve: (a) Ir foil, (b) commercial $IrCl_3$, (c) precalcined commercial IrO_2, (d) IrO_x/C, (e) IrO_x/Com. ATO and (f) IrO_x/ATO.*

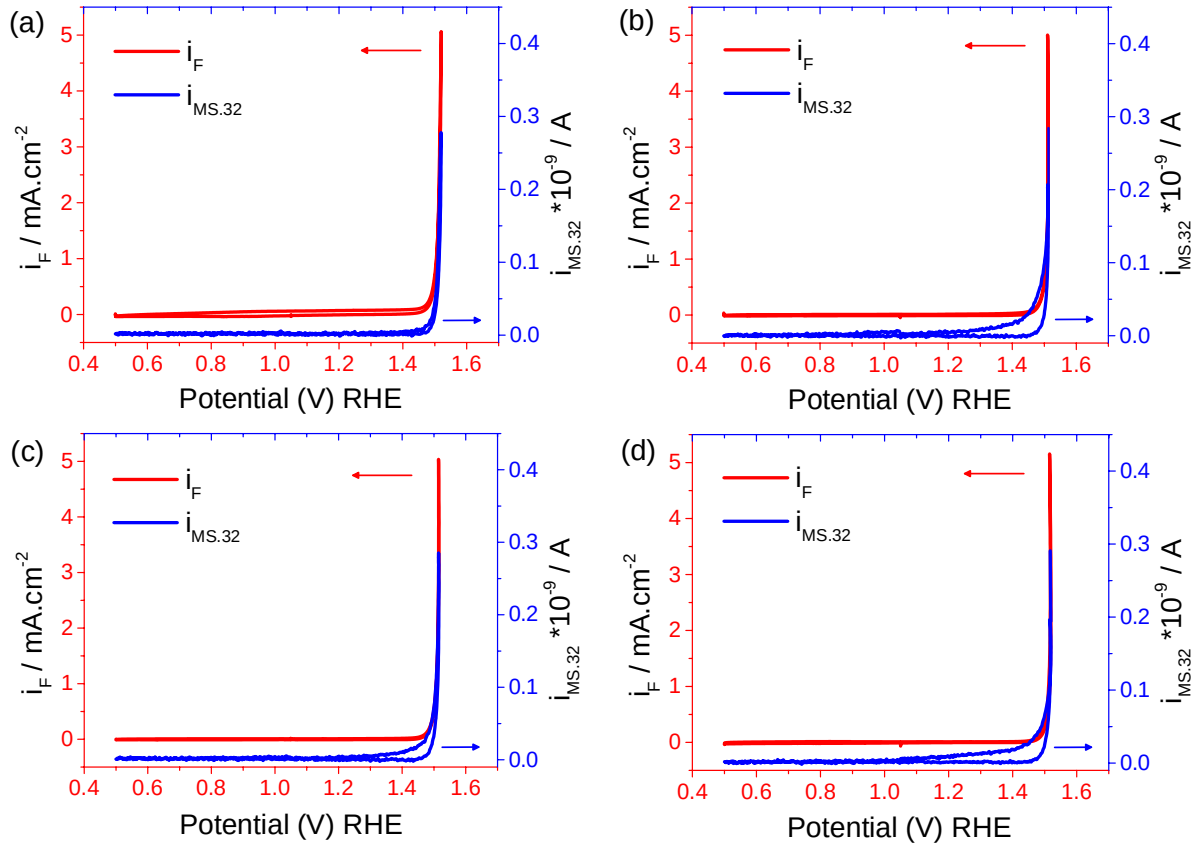

Figure S6. *Simultaneously recorded cyclic voltammgorams (CV) and mass spectrometric cyclic voltammograms (MSCV) for oxygen evolution reaction (OER) in N_2 saturated 0.05 M H_2SO_4 solution in the* dual thin-layer electrochemical flow cell. *(a) bulk IrO_x, (b) IrO_x/C, (c) IrO_x/Com. ATO and (d) IrO_x/ATO.*

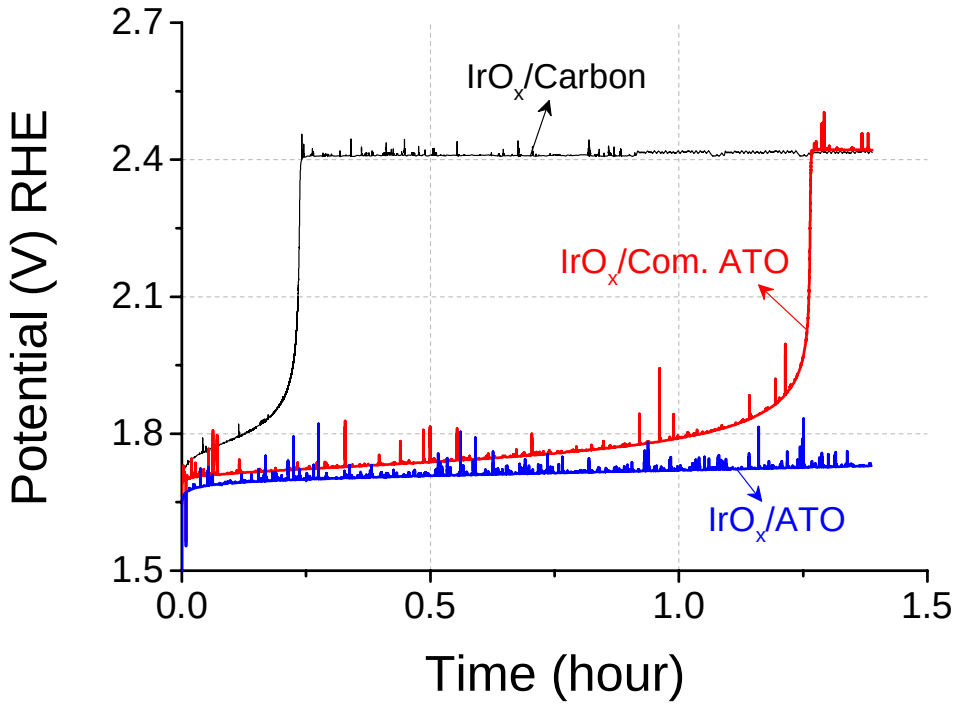

Figure S7. *10 mA cm^{-2} constant current-load stability test of IrO$_x$/ATO electrocatalysts for OER. For comparision, IrO$_x$/C and IrO$_x$/Com. ATO measured under same condition. Ir electrocatalyst loading 10.2 μg cm^{-2}, N$_2$ purged 0.05 M H$_2$SO$_4$ (pH 1), 1600 rpm, room temperature.*

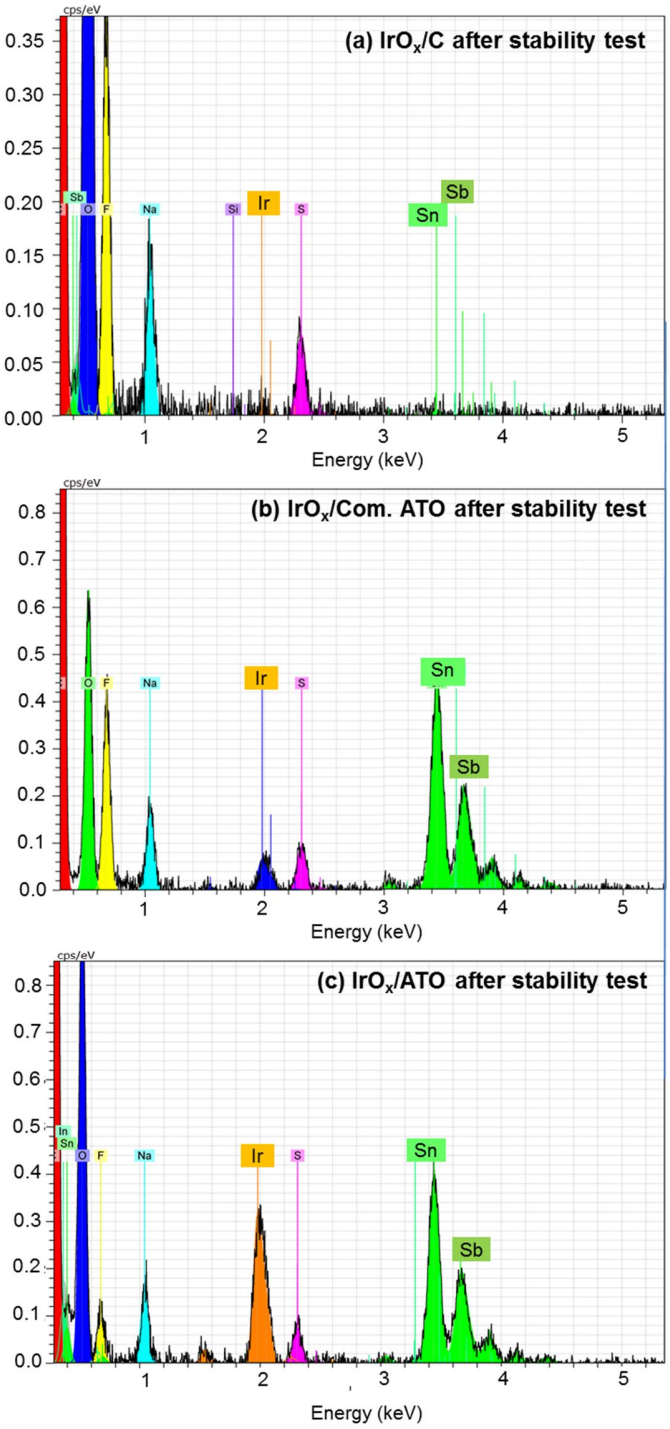

Figure S8. *EDX patterns of IrO_x nanoparticles supported on (a) carbon black, (b) commercial ATO and (c) synthesized ATO after stability test.*

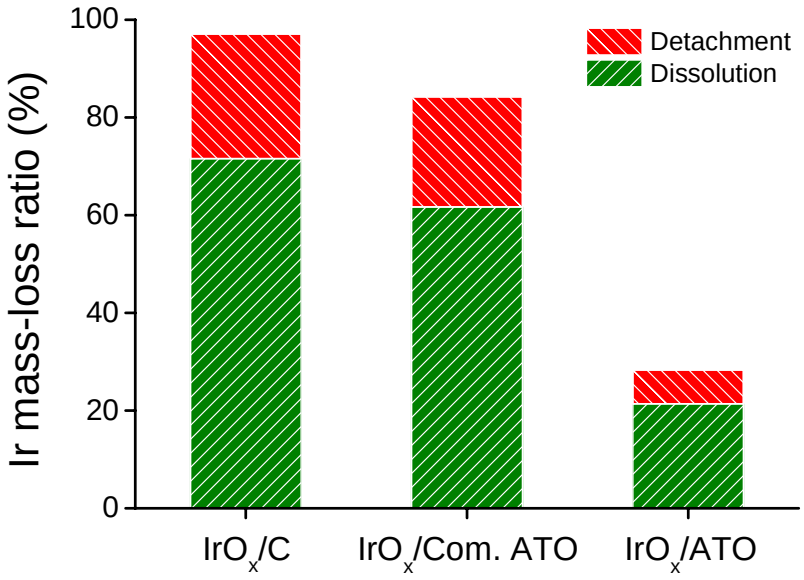

Figure S9. *Ir-mass loss ratio of IrO_x/C, IrO_x/Com. ATO and IrO_x/ATO after stability test based on the initial Ir mass. Red and Green portions indicate the nature of the Ir loss, by detachment or by dissolution.*

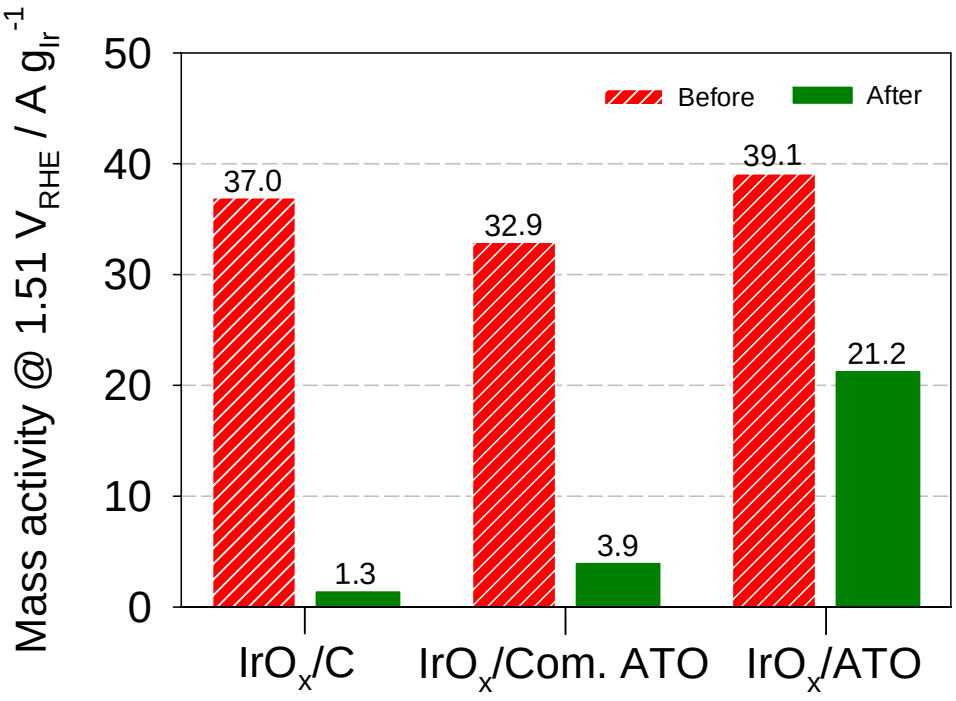

Figure S10. *Ir-mass based activity at η = 280 mV overpotential of IrO_x/C, IrO_x/Com. ATO and IrO_x/ATO before and after stability test. The mass activity of reference catalysts (IrO_x/C and IrO_x/Com. ATO) before stability test was similar with our previous report (H. N. Nong and P. Strasser etc., Angewandte Chemie International Edition 2015, 54, 2975-2979).*

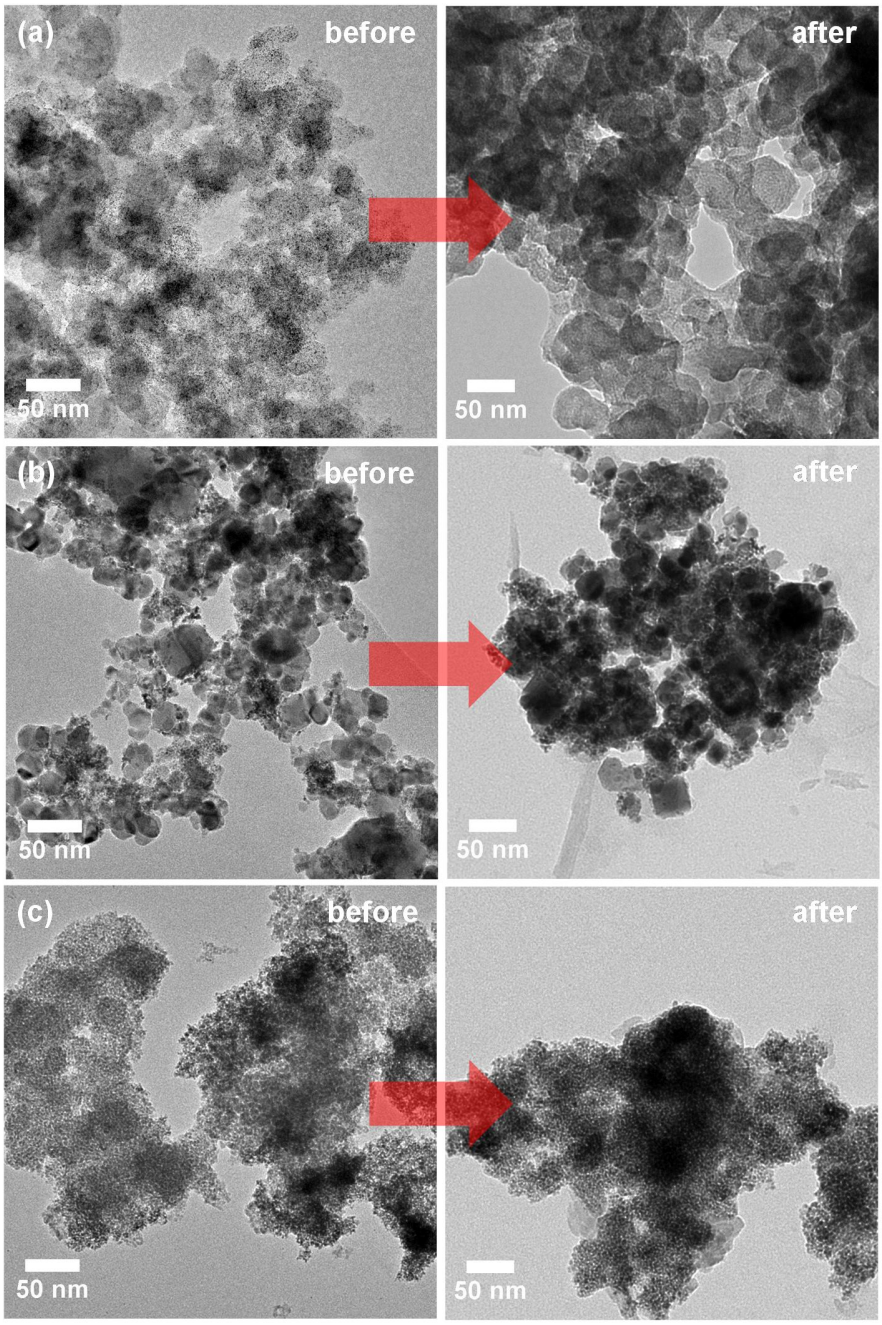

Figure S11. *TEM images of IrO_x nanoparticles supported on (a) carbon black, (b) commercial ATO and (c) synthesized ATO before and after stability test.*

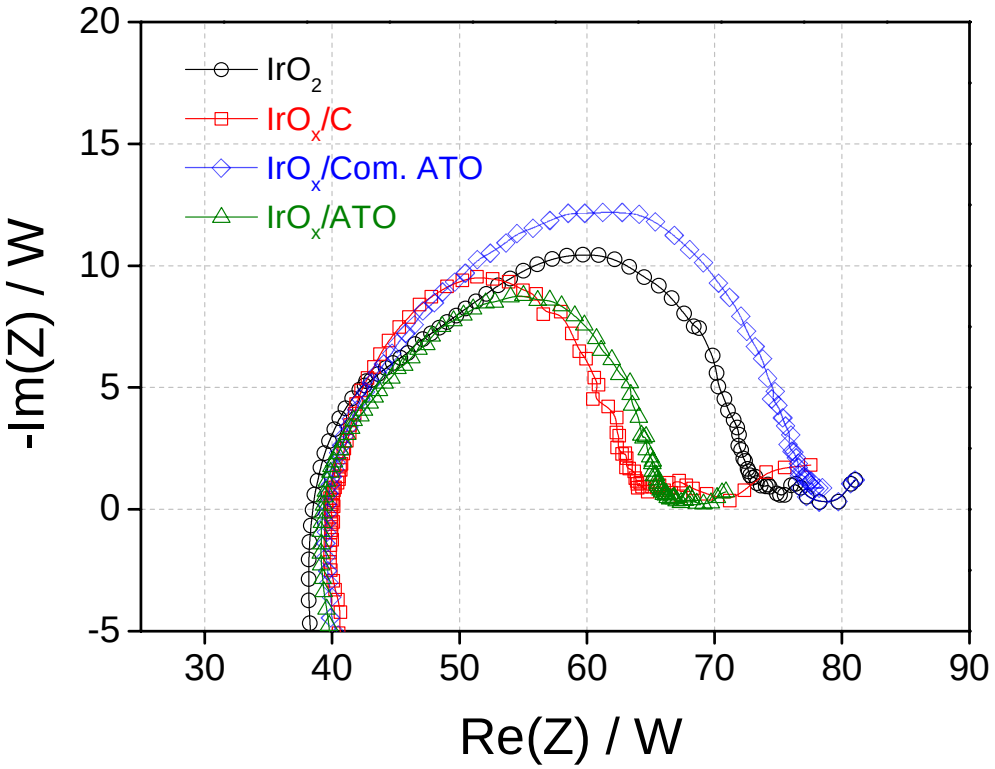

Figure S12. *Nyquist plots of commercial IrO_2, IrO_x/C, IrO_x/Com. ATO and IrO_x/ATO at 1.7 V_{RHE}, Ir electrocatalyst loading 10.2 μg cm^{-2}, N_2 purged 0.05 M H_2SO_4 (pH 1), 1600 rpm, room temperature, frequency range 1 Hz ~ 100 kHz.*

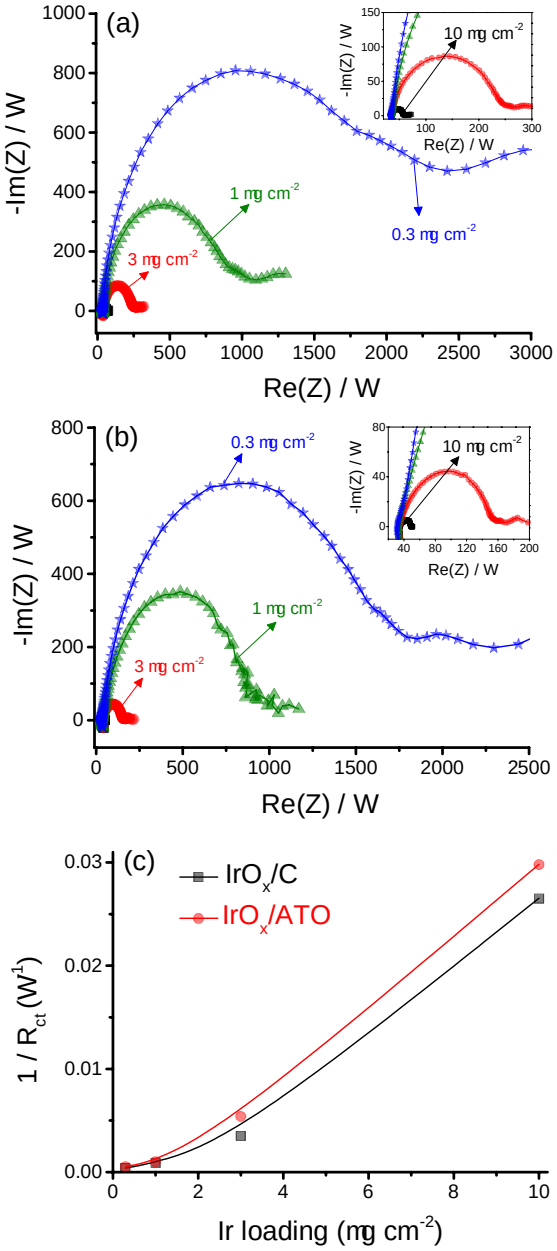

Figure S13. *Nyquist plots of (a) IrO_x/C and (b) IrO_x/ATO at 1.7 V_{RHE} with different Ir electrocatalyst loading (10, 3, 1 and 0.3 $\mu g_{IrO_x}\ cm^{-2}_{geo}$). (c) Charge transfer resistance of IrO_x/C and IrO_x/ATO as a function of Ir electrocatalyst loading. N_2 purged 0.05 M H_2SO_4 (pH 1), 1600 rpm, room temperature, frequency range 1 Hz ~ 100 kHz.*

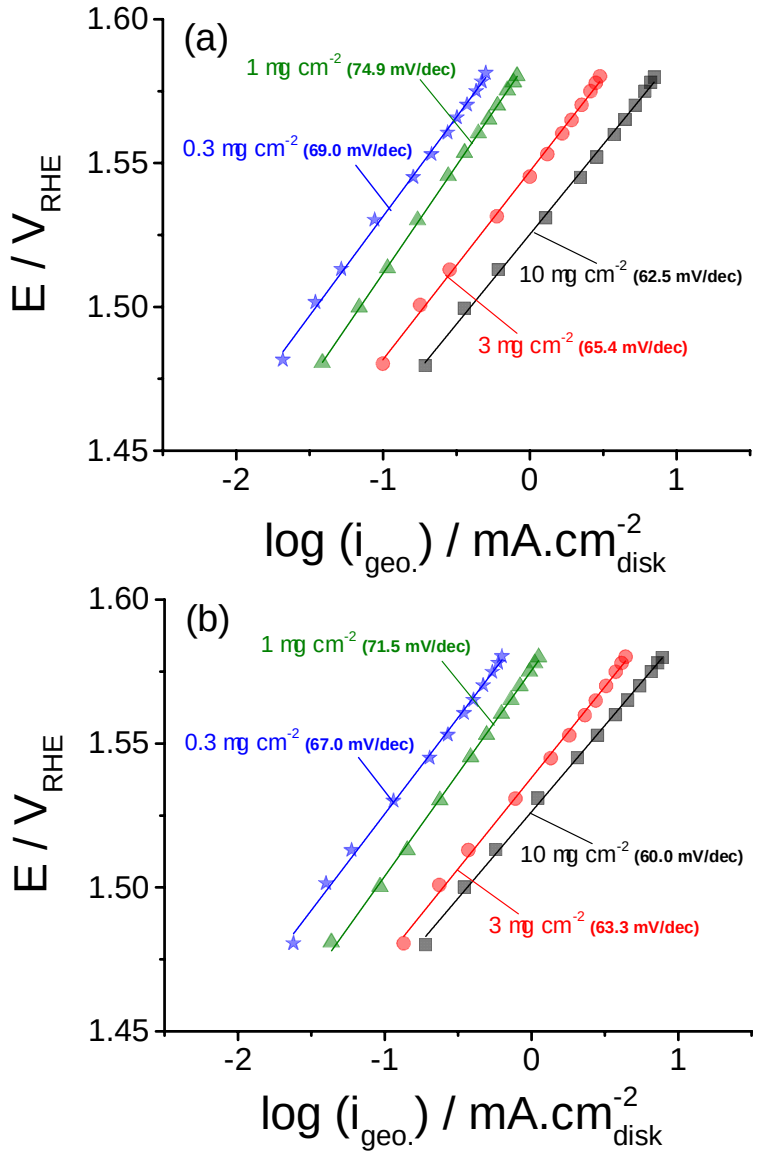

Figure S14. *Tafel plots of (a) IrO_x/C and (b) IrO_x/ATO with different Ir electrocatalyst loading (10, 3, 1 and 0.3 $\mu g_{IrO_x}\ cm^{-2}_{geo}$). N_2 purged 0.05 M H_2SO_4 (pH 1), scan rate 5 mV s^{-1}, 1600 rpm, room temperature, To calculate the tafel slope, 12 data points took in iR-corrected 1.45 ~ 1.60 V_{RHE}.*